Semiconductor Physics, Quantum Electronics & Optoelectronics, 2024. V. 27, No 1. P. 040-053.

Structure and optical characterization of chitosan-chitin/Ag nanocomposite thin films

T.O. Malakhovska[1], A.I. Pogodin[1], M.J. Filep[1,2], R. Mariychuk[3], M.M. Pop[1], Ya.I. Studenyak[1], V.V. Vakulchak[1], V. Komanicky[4], S. Vorobiov[4], M.Yu. Sabov[1]

[1]*Uzhhorod National University, 46, Pidhirna str., 88000 Uzhhorod, Ukraine*
[2]*Ferenc Rakoczi II Transcarpathian Hungarian Institute, Kossuth Sq. 6, 90200 Beregovo, Ukraine*
[3]*University of Presov, Faculty of Humanity and Natural Sciences, Department of Ecology,*
17th November 1, 08116 Presov, Slovakia
[4]*P.J. Šafarik University, Institute of Physics, Faculty of Science, Park Angelinum 9, 04154 Kosice, Slovakia*
**Corresponding author e-mail: t.malakhovska@gmail.com*

Abstract. Chitin and its derivatives are common natural polymers that are widely used in various technological fields. In recent years, considerable attention has been paid to the preparation of polymer nanocomposites based on metal nanoparticles (NPs). Chitin/chitosan-based composites due to high antibacterial activity are suitable for application in related food storage, textile industries. This paper presents an effective and simple method of obtaining chitosan-chitin copolymer/Ag nanocomposites with an extremely high content of metal nanoparticles. The structure and morphology of the synthesized nanocomposites were investigated using X-ray diffractometry, Fourier-transform infrared spectroscopy, electron microscopy, and their optical properties were studied using UV-VIS spectroscopy as well as spectral ellipsometry. It was ascertained that the resulting nanocomposite films are characterized by a uniform distribution of spherical silver nanoparticles, the sizes of which increase (from 55 up to 143 nm) with increasing the Ag^+-ions concentration in the reaction mixtures. The optical absorption spectra of nanocomposites are characterized by the presence of an absorption maximum within the range 458…525 nm, which confirms the formation of Ag NPs. A monotonous increase in the values of the energies of optical transitions was observed in the process of increasing the average size of NPs.

Keywords: nanocomposite, chitosan, optical properties, electron microscopy, X-ray diffractometry.

https://doi.org/10.15407/spqeo27.01.040
PACS 36.20.Kd, 36.20.Ng, 68.55.am

Manuscript received 10.10.23; revised version received 24.12.23; accepted for publication 28.02.24; published online 12.03.24.

1. Introduction

Nanoparticles (NPs) are a wide class of materials that attract considerable attention due to the great variability of compositions, the significant dependence of properties on the structure of the particle, its morphology, and synthesis methods. This leads to a wide area for promising use of nanoparticles, which is not limited only to technologies based on their physical properties – magnetic, optical, electrical, *etc*., but also opens up prospects for the use of NPs as catalysts, biosensors, in medicine (antibacterial and antifungal agents, diagnosis of diseases, drug delivery), agriculture, food technology, *etc*. [1–4]. Wide commercial use of nanomaterials – from products of daily use (creams, polymer fillers, coatings) to energy-saving and energy conversion technologies [3–6], encourages further research in the field of nanomaterials.

Among inorganic nanoparticles, a consistently high scientific and practical interest in various types of metal NPs [7], primarily in NPs based on Ag [8], Pt [9], Au [10], Cu [11] remains stable, which is related to the high bioactivity of these elements. The advantages of these metals are low toxicity, stability in aqueous/non-aqueous solutions, ability to functionalize NPs depending on needs. Commercially, Ag NPs are the most common, which is related to both the availability of this metal and the unique properties of Ag NPs. Thanks to the well-known characteristics of localized surface plasmon resonance (LSPR), Ag NPs have clear absorption bands, the location of which is regulated by the size and morphology of the particles, which is often used in the manufacture of optical sensors [12]. Clearly expressed antibacterial properties of Ag NPs lead to their use in water purification, food storage, textile industry [13–15]. The high conductivity of Ag NPs is the basis for production of conductive inks and flexible electronics, anodes in Li-ion batteries [16, 17].

As it was mentioned, the size and morphology of NPs are sensitive to the conditions of synthesis – temperature, used reducing agent and stabilizer, which is related to a significant number of studies. Most often, chemical reduction or various techniques of photo-chemical and electrochemical effects are used to prepare Ag NPs [1–3]. However, the constant increase in the need to produce NPs, along with their high price and the use of dangerous reagents, leads to the development of such technologies as green synthesis and biochemical techniques [18–20]. The green synthesis, due to its greater availability, provides an alternative to the use of expensive reagents, which contributes to expansion of the application limits for obtaining the nanomaterials.

Nanomaterials owe to the manifestation of new and better properties, as compared to bulk phases, due to their extremely small size (<100 nm), a large number of boundary atoms and high surface energy. But this is also their biggest problem, since NPs are thermodynamically unstable and prone to spontaneous aggregation [21]. To increase the stability of NPs, various substances are used – stabilizers, which include both low-molecular compounds and polymers [22, 23]. The use of polymers to produce nanomaterials not only provides high stability due to significant coverage of the NPs surface (steric factor), but also enables the use of the polymer as a matrix for obtaining a new class of nanomaterials – polymer nanocomposites [24]. Nanocomposites are heterophase multicomponent materials in which inorganic NPs are distributed in an organic matrix. Such a structure makes it possible to obtain new materials that combine the properties of all constituent parts, and it is also possible to strengthen the properties of both components (synergism) [24]. The possibility of modifying the structure of polymers, due to introduction of new functional groups, allows to change the necessary properties in a controlled manner (lyophobic/lyophilic surface properties, optical, electrophysical and mechanical parameters) to obtain new materials with specialized properties. A feature of polymer nanocomposites is their flexibility, which opens up new opportunities in the field of wearable electronic devices [24].

Stabilization with the help of biopolymers and formation of polymer nanocomposites with their participation fully falls under the concept of green chemistry, since there are a large number of macromolecules in nature. They are distinguished by their availability, cheapness, biodegradability and non-toxicity [25]. Among biopolymers – polysaccharides, polypeptides and polynucleotides – the first are the most common in nature [26]. It is worth noting that the most common polysaccharide of plant origin is cellulose. Next is a cellulose-like polymer of animal origin – chitin $(C_8H_{13}O_5N)_n$ (N-acetylglucosamine), which is part of the outer shell of all arthropods and the cell walls of fungi [27]. Chitin has a rigid polymer frame and is not soluble in water, but only in strong acids, but the dissolution process is accompanied by its decomposition. By deacetylation of chitin, a new aminopolysaccharide – chitosan (2-amino-2-deoxy-beta-D-glucan) is obtained, which, unlike chitin, is soluble in dilute acids (HCOOH, CH_3COOH) [28]. Chitosan has biological activity, in particular, antibacterial properties, which are used in the food, medical, cosmetic industry and in water purification. A useful property of chitosan is the possibility to obtain it in the form of nanoparticles, films, fibers, gels, membranes, sponges [28, 29].

Active researching the nanocomposites based on chitosan and Ag NPs is reported. Considering the high bioactivity and possible synergism of the properties of chitosan and Ag NPs, a number of publications refers to the research of antibacterial and antifungal drugs [30], for use in water purification [31] and in the textile industry [32]. Also, the chitosan/Ag NP composites demonstrate a high antioxidant activity [33]. The combination of chitosan's flexibility with electrical conductivity of silver in nanocomposites is used in wearable electronic technology, conductive inks, and sensors [34, 35]. However, it should be noted that the research data refer to a limited concentration range (up to 20% Ag NPs). The chitin and Ag NPs based composites [36], similar to the chitosan-based ones, also show an antibacterial property. Besides, an anti-cancer activity of both chitosan/Ag NPs and chitin/Ag NPs composites have been reported [33]. Additionally, the synthesis of these nanocomposites was carried out by mixing already obtained Ag NPs with organic matrix.

Therefore, taking into account the significant interest in researching new nanocomposite materials based on chitosan and Ag NPs, we decided to study and develop a simple technology for preparation of a chitosan-chitin copolymer/Ag nanocomposite in a wide concentration range and to ascertain the effect of the concentration and size of Ag NPs on the structural and optical properties of the obtained nanocomposites.

2. Experimental

2.1. Sample preparation

High purity substances were used for the research: chitosan (degree of deacetylation 91.6%), silver nitrate ($AgNO_3$ 99%), ammonium solution (NH_4OH 25 wt.%), glacial acetic acid (CH_3COOH 99.8%), ascorbic acid ($C_6H_8O_6$ 99.5%). The source solutions (1.67 wt.% silver nitrate, 0.87 wt.% ascorbic acid, 10 wt.% acetic acid, 10 wt.% ammonium solution) were prepared using the distilled water.

Powdered chitosan ($m \sim 0.25\ldots1$ g) was dissolved in 10 wt.% acetic acid (continuous stirring at the temperature $T = 25$ °C) resulting a gel-like homogeneous solution. It is obvious that the dissolution of chitosan is not a physico-chemical process, *i.e.*, formation of chitosan acetate (Ch-Ac) (Eq. (1)) occurs [37].

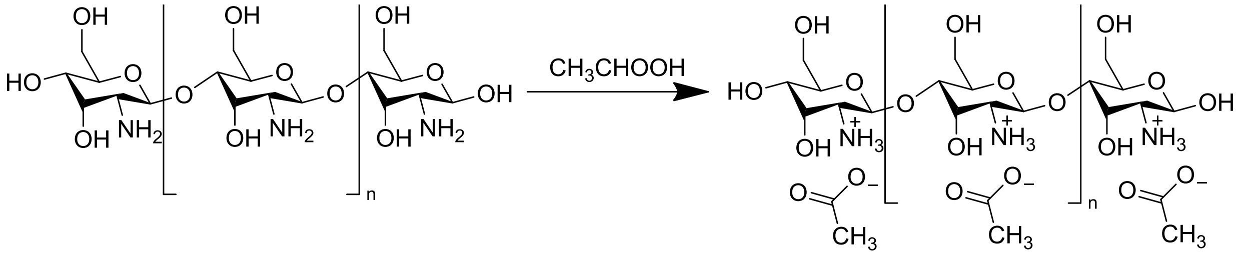

(1)

The required amount of AgNO$_3$ solution was added to the obtained gel-like Ch-Ac solution. Ag$^+$ was reduced with a 0.87 wt.% ascorbic acid solution (Eq. (2)) at the rate of 0.02 cm^3·min^{-1} by using continuous stirring with a magnetic stirrer at the temperature 25 °C.

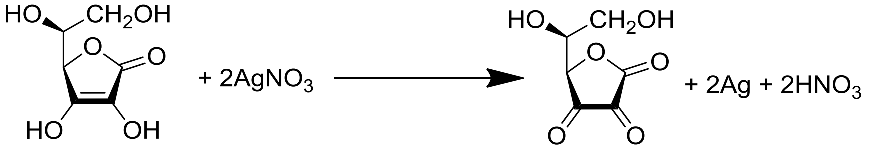

(2)

This mode contributed to the release of silver in the form of NPs, with a small degree of aggregation [37].

In the process of reducing Ag$^+$ to Ag^0, in the incident light, a gradual change in the color of the reaction mixtures was observed: yellow (9 wt.% Ag^0) → red (15…22 wt.% Ag^0) → light green (> 22 wt.% Ag^0). The completeness of the chemical reaction is proven by the absence of Ag$^+$ ions in the solution (absence of a white precipitate of AgCl when KCl is added). To obtain the composite based on chitosan and Ag NPs (Ch-Ag NPs) in a dry form, the necessary amount of 10 wt.% ammonia solution was added to the reaction mixture, which is necessary for neutralization of acetic acid and destruction of the Ch-Ac salt (Eq. (3)). Subsequently, the precipitated Ch-Ag NPs composites were washed with double distilled water to a neutral reaction, and dried in air at the temperature 25 °C.

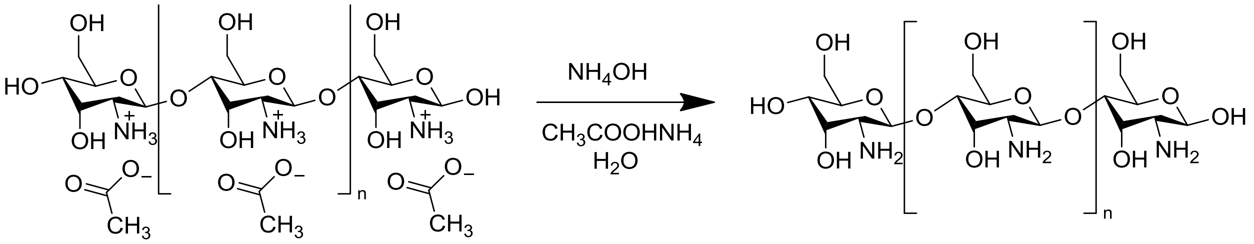

(3)

To obtain thin films of Ch-Ag NPs composites, the latter were dissolved in a 10 wt.% acetic acid solution to prepare gel-like solutions. All composite films were prepared using the same technique that consisted of spontaneous spreading 0.1 cm^3 of gel onto the substrate and then slowly drying the resulting film. The drying was performed in air at 25 °C. As a result, thin films of chitosan-chitin copolymer with silver nanoparticles (Ch-Chn-Ag NPs) were obtained, both on substrates (glass and silica) and in a separate form, with a mass concentration of Ag^0 (calculated) in the range of 9 to 80 wt.%.

2.2. Methods

To confirm the composition of the organic matrix in the film of the obtained Ch-Chn-Ag NPs composites, the Fourier transform infrared method with attenuated total reflection (ATR–FTIR) was used. Spectra of films of Ch-Chn-Ag NPs composites were obtained using Shimadzu Prestige 21 spectrometer with ATR ZnSe. The FTIR spectra were collected in the 600…4000 cm^{-1} range in transmittance mode. The measurements were performed in air atmosphere with applied correction of the CO$_2$ and H$_2$O peaks.

The analysis of the phase composition of the obtained Ch-Chn-Ag NPs composites was carried out using an AXRD diffractometer equipped with linear Si-strip detector (DECTRIS MYTHEN2 R 1D) and CuK$_\alpha$ radiation (Ni – filter) in the Bragg–Brentano geometry (θ/2θ angles scanning mode). The scanned range was $10° \leq 2\theta \leq 90°$ with exposition 1 s per step. The phase analysis and calculating of peaks broadening were performed using the PDAnalysis (Proto Manufacturing) software.

The study of the microstructure of Ch-Chn-Ag NPs composites, in order to determine the size of nanoparticles and their distribution in polymer matrices, was carried out using the method of electron microscopy (SEM Vega Tescan 3 (secondary electron, backscattered-electron (SE, BSE) detectors, applied accelerating voltage was 30 kV, working distance around 10 mm, the view field 7.25 μm^2). Composition and elemental analysis of the samples was made using the scanning electron microscope (SEM) equipment (Tescan VEGA3) with an energy dispersive X-Ray (EDX) detector (Oxford Instruments) to determine elemental composition. The analysis of SEM images was carried out in AmScope 4.8.

The experimental data of absorption (transmission) spectra of Ch-Chn-Ag NPs films on a silica substrate (relatively to silica substrate – pure polymer film) were obtained using a Shimadzu UV-2600 UV–VIS spectrophotometer (detectors: photomultiplier and semiconductor InGaAs, spectral range: 190…1100 nm, 1 nm scan step, UVProbe software equipped with an ISR-2600Plus integrating sphere.

The dispersion of refractive index *n* and the extinction coefficient *k* of Ch-Chn-Ag NPs composite films was studied with a HORIBA Smart SE spectral ellipsometer within the spectral range 440…1000 nm, at the angle 70°.

3. Results and discussion

3.1. Structure

On the FTIR spectra of the pure Ch-Chn composite film (without Ag NPs) in the range 600…4000 cm^{-1}, characteristic bands with the following values are observed (Fig. 1a): the band at 897 and 945 cm^{-1} corresponds to the deformation vibrations of the C–H groups, which are present in the structure of polysaccharides, in the region of their fingerprints, the bands at 1153, 1069 and 1026 cm^{-1} correspond to valence vibrations of the C–O group (asymmetric valence vibrations of C–O–C of the pyranose ring or –C–OH glycosidic hydroxyl), 1660 cm^{-1} – vibrations of the –C=O group. The available reflection bands from 2926 to 2876 cm^{-1} correspond to valence vibrations of –CH$_2$ and have a relatively low intensity. In the high-frequency part of the spectrum (2950…3700 cm^{-1}), the interpretation is complicated because of the superimposition of bands of valence vibrations of the hydroxyl group and deformation vibrations of the amino group. Namely, broad reflection bands of free, associated and hydrogen-bonded –OH groups and bands corresponding to asymmetric and symmetric valence vibrations of the amino group appear. The characteristic broad band at 2926…2876 cm^{-1} corresponds to the C–H valence vibrations of the methylene group.

However, although the FTIR spectra of the film show vibrations of groups typical for chitosan [38], the diffractogram of the film (Fig. 1b) shows the presence of high-intensity peaks that are not characteristic of the chitosan structure [38]. This may be related to obtaining a polymer film not of pure chitosan, but of a chitosan-chitin copolymer [39].

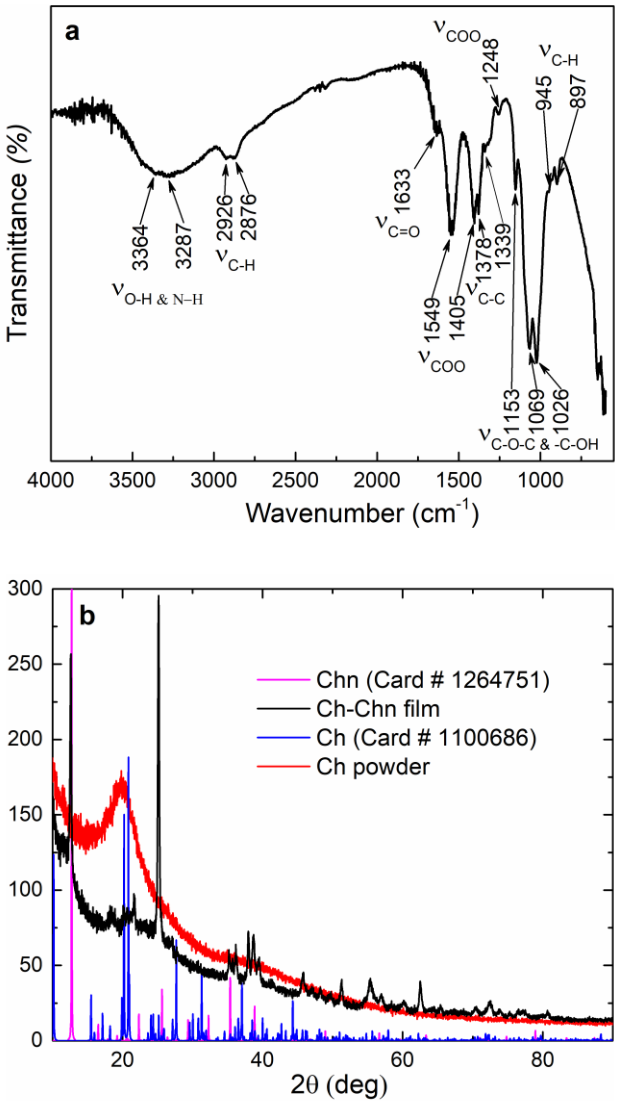

Fig. 1. FTIR spectrum of the pure chitosan-chitin copolymer film of Ch-Chn polymer (a), comparison of diffractograms of powdered chitosan Ch (red line) and thin film of Ch-Chn (black line) based on it. (Color online)

Chitin and chitosan are related biopolymers with a glucosamine framework. The structural difference between them is the presence of an acetyl group at the nitrogen atom. The process of acetylation, *i.e.*, the conversion of chitosan to chitin, is relatively easy in the presence of acids. Opposed to deacetylation process, which usually requires harsh reaction conditions. That is, drying the chitosan solution applied to the substrate in acetic acid may contribute to the partial acylation of amino groups. Formation of chitosan-chitin copolymer is shown in Eq. (4).

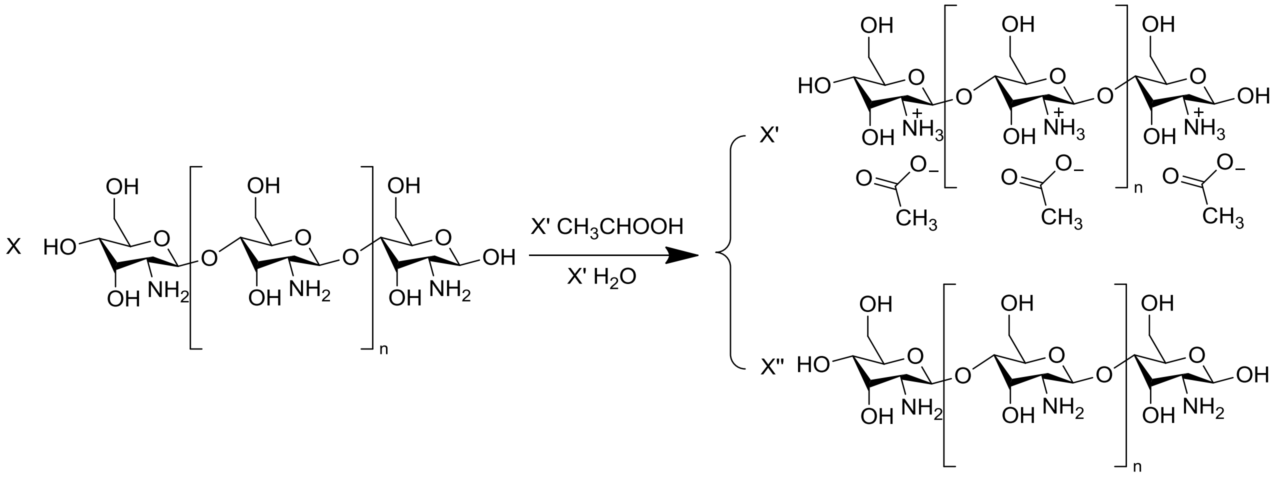

(4)

In the IR spectra of Ch-Chn-Ag NPs composites, no additional vibrations are observed, which indicates the absence of new chemical bonds. That is, polymerization in the presence of Ag NPs does not lead to a change in the structure of the polymer matrix. Only a significant decrease in the intensity of the bands corresponding to the characteristic vibrations of groups corresponding to the structure of polysaccharides (Fig. 2a blue color) and carboxylic acid groups (Fig. 2a yellow color) is observed in the process of increasing the concentration of Ag NPs in the obtained composite. Moreover, at high concentrations of silver (71 wt.%, 80 wt.%), vibrations and groups of the polymer are not practically observed.

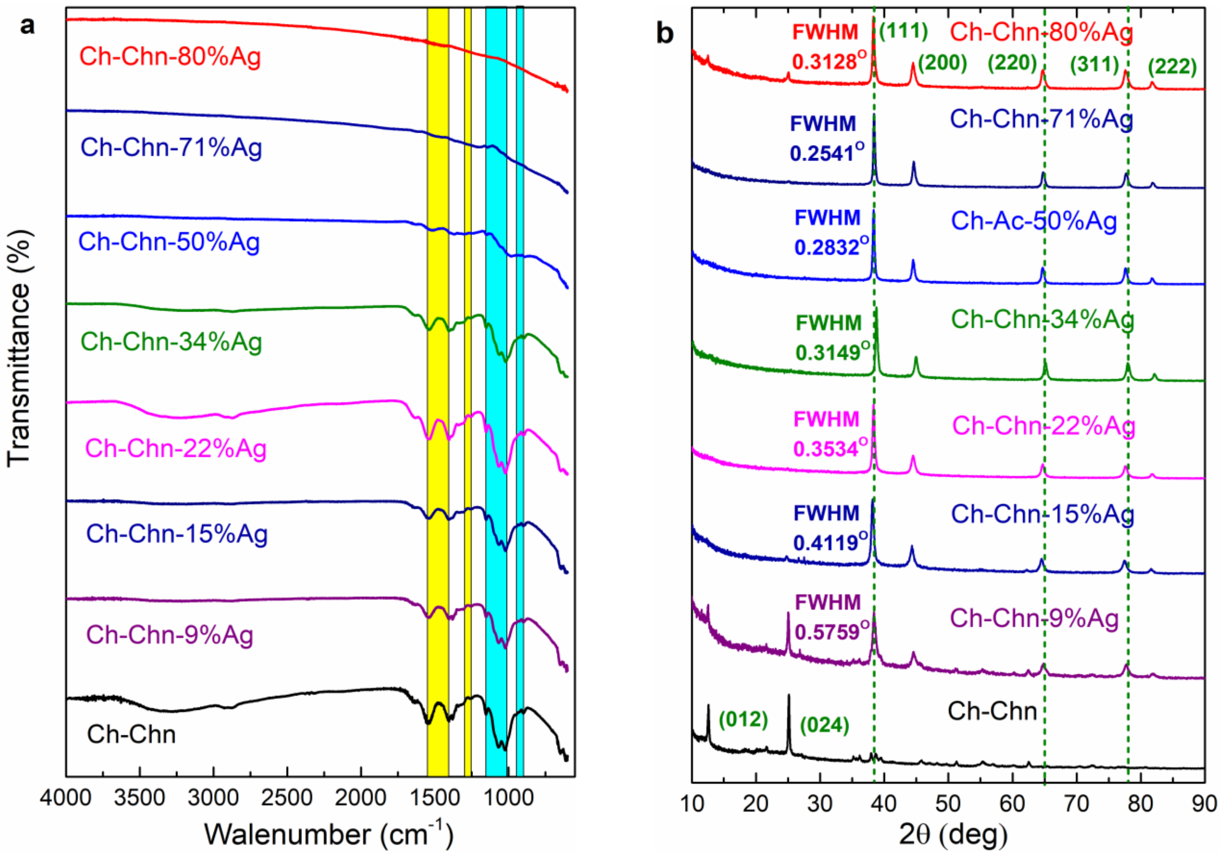

Fig. 2. Comparison of FTIR spectra (a) and diffraction patterns (b) of Ch-Chn-Ag NPs composites ((*hkl*) for silver and chitin planes are marked by green and blue, respectively). (Color online)

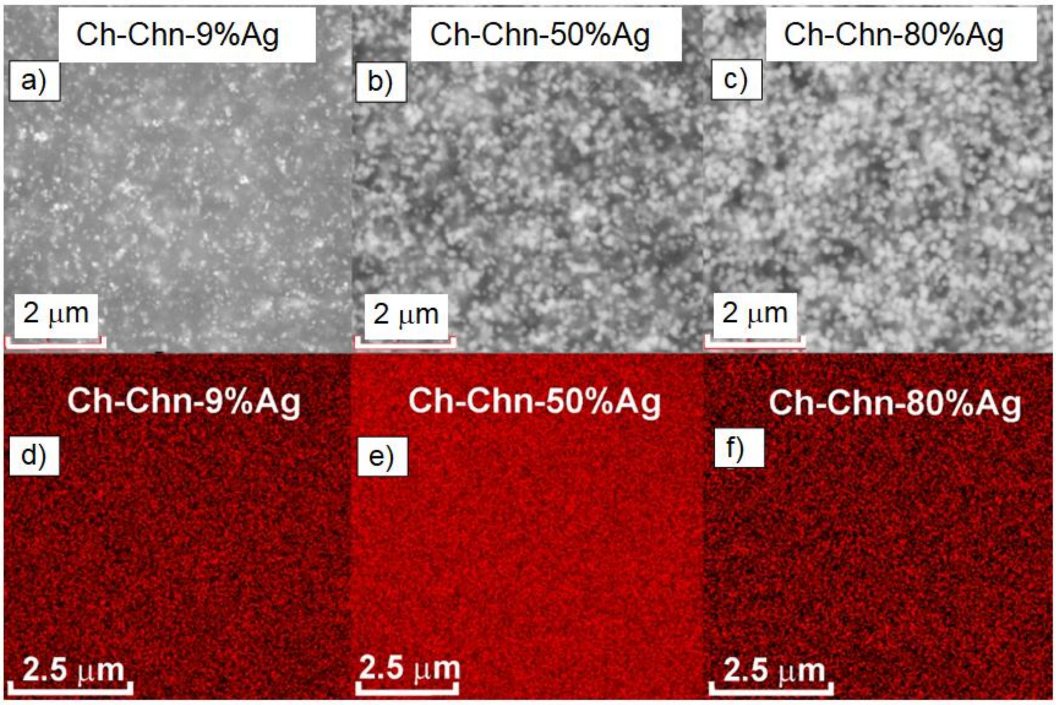

Fig. 3. SEM images (a, b, c) and EDS maps (d, e, f) of silver on the example of some composites.

By comparing the diffractograms of Ch-Chn-Ag NPs composites with different concentrations (Fig. 2b), a gradual increase in Ag-peak intensities (planes (111), (200), (220), (311) and (222)) was revealed in the process of increasing its concentration in the composite with a simultaneous decrease in their broadening. The broadening of peak was estimated by calculating the full width at half maximum (FWHM). The corresponding peaks were fitted by the Gauss function. The values of FWHM were observed for the silver most intensive peak, which correspond to the plane (111). A fairly sharp decrease in the FWHM values is observed within the concentration range of 9 to 22 wt.% Ag^0, while a further increase in the silver content leads to a gradual slight decrease (with a slight increase in FWHM for the composite with the concentration of Ag^0 80 wt. %). At the same time, a decrease in the intensity of the polymer matrix reflexes is observed, which are almost absent in the diffractograms with Ag NPs concentration > 15 wt.%. However, for the Ch-Chn-Ag NPs composite with the Ag^0 concentration close to 80 wt.%, the reflexes of the chitin-chitosan copolymer appear again, which is possibly related to the peculiarity of the film morphology.

3.2. Microstructure

The study of the silver nanoparticles microstructure and their distribution in the obtained Ch-Chn-Ag NPs composites was carried out using the electron microscopy (SEM) technique. Formation of spherical silver nanoparticles was ascertained due to analysis of SEM images (Figs 3a–3c). No any formation of other shapes inherent to NPs was recorded. Only the Ag NPs aggregation effect is observed in the process of increasing their concentration in the composite, which is indicated by the increase in the size of the spheres. It should be noted the high uniformity of Ch-Chn-Ag NPs films, which is indicated by the uniform distribution of Ag on the EDS maps (Figs 3d-3f).

At the same time, the Map sum EDS spectrum of Ch-Chn-AgNPs composites (Fig. 4) obtained from a film area of 7.25 μm^2 shows, along with the reflexes corresponding to silver nanoparticles, the reflexes of carbon and oxygen, which correspond to the organic matrix. The absence of nitrogen reflexes is noteworthy, which is caused by its low concentration in the polymer matrix (one nitrogen atom per monomer unit).

Let us consider in more detail the effect of silver concentration on the Ag NPs aggregation process in composites. To make it, we would first consider the histograms of Ag NPs size distribution (Fig. 5). It was found that at relatively small concentrations of silver (9…22 wt.%), a significantly narrower range of particle size distribution (~20…165 nm) is observed. The further increase in the concentration of Ag^0 (from 34 wt.%) leads to a sharp expansion of the distribution range. At the same time, there is a decrease in the number or even absence of nanoparticles with a size of < 50 nm and, instead, the appearance of particles with the diameter of up to 300 nm (Fig. 5). It is obvious that this is a consequence of aggregation phenomena, which are intensified due to the decrease in the distance between Ag^0 particles in the composite due to the increase in their concentration.

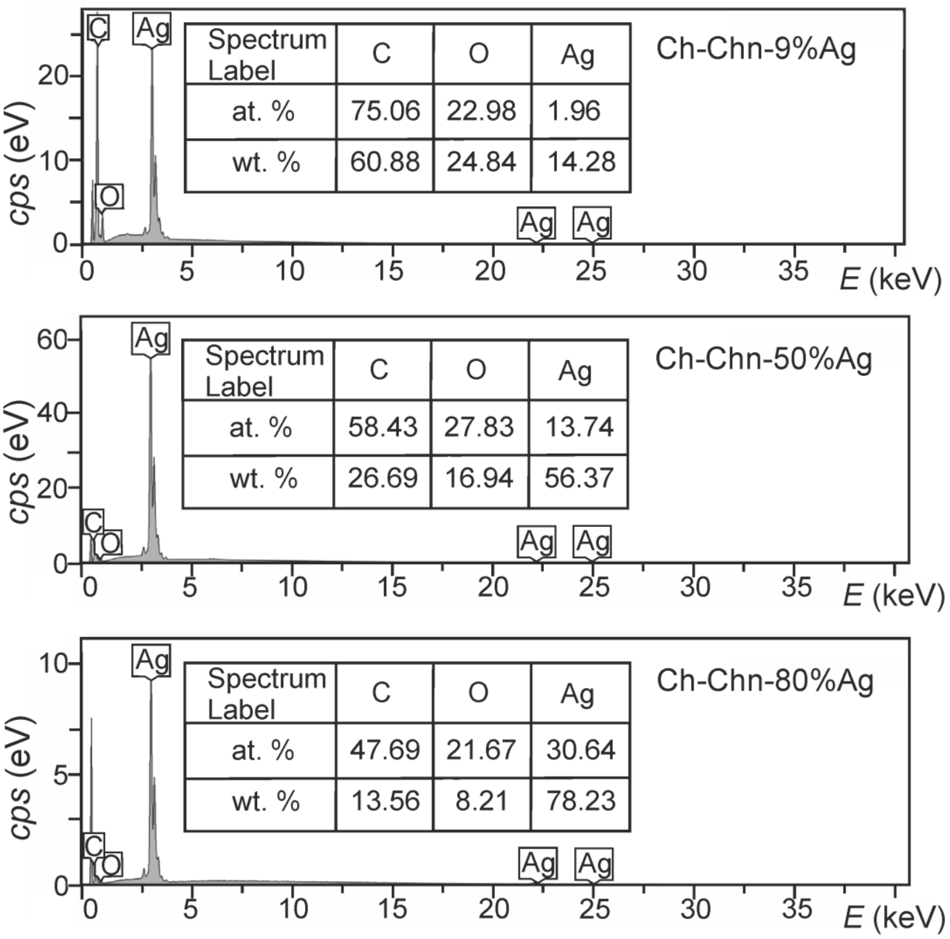

Spectrum Label	C	O	Ag
at. %	75.06	22.98	1.96
wt. %	60.88	24.84	14.28

Spectrum Label	C	O	Ag
at. %	58.43	27.83	13.74
wt. %	26.69	16.94	56.37

Spectrum Label	C	O	Ag
at. %	47.69	21.67	30.64
wt. %	13.56	8.21	78.23

Fig. 4. Map sum EDS spectrum of Ch-Chn-Ag NPs on the example of some composites.

Also, an increase in the concentration of Ag^0 leads to an increase in the average size of nanoparticles (Figs 5 and 6) from 55 to 143 nm. It was ascertained that the compositional dependence of the average size of crystallites (Fig. 6) has a monotonous nonlinear character.

At relatively low concentrations of silver (9…22 wt.%), a slight change in the average size of the particles is observed due to sufficiently large distances in the composite between them. A decrease in the distance between particles causes a sharper increase in their average size (22…50 wt.%). Further slowing of the particle size increase rate in composites with the concentration 71…80 wt.% is associated with formation of significant aggregates with lower free surface energy than the weakly aggregated ones.

3.3. Optical properties

The obtained experimental spectra of the refractive index *n* (Fig. 7a) and the extinction coefficient *k* (Fig. 7b) were analyzed using the DeltaPsi2 software by using the Drude and Tauc–Lorentz models for the layer of silver nanoparticles and the classical model for the polymer. It enabled to describe the spectral dependence parameters Δ and Ψ for thin metal films and determine other optical parameters with high accuracy [42]. The model consisted of layers of substrate-polymer-silver nanoparticles-polymer (roughness).

It was ascertained that the dispersion of the refractive index and the extinction coefficient of the polymer films with different silver content is characterized by the presence of a slight maximum in the spectral region of 500 to 700 nm, while for the pure polymer, both *n* and *k* change almost linearly in the entire studied spectral range. It is also possible to observe an increase in the values of the refractive index and the extinction coefficient with an increase in the content of silver in the polymer.

As a result of the analysis aimed at the dispersion of the refractive index and the extinction coefficient, the thickness of the films of Ch-Chn-Ag NPs composites were determined using the aforementioned models (Ch-Chn = 8 μm, Ch-Chn-Ag NPs 9% = 34 μm, Ch-Chn-Ag NPs 15% = 44 μm, Ch-Chn-Ag NPs 22% = 24 μm, Ch-Chn-Ag NPs 34% = 35 μm, Ch-Chn-Ag NPs 50% = 30 μm, Ch-Chn-Ag NPs 71% = 10 μm, Ch-Chn-Ag NPs 80% = 10 μm). The content of Ag^0 in the composites was also estimated: Ch-Chn-Ag NPs 9% = 9.5%,

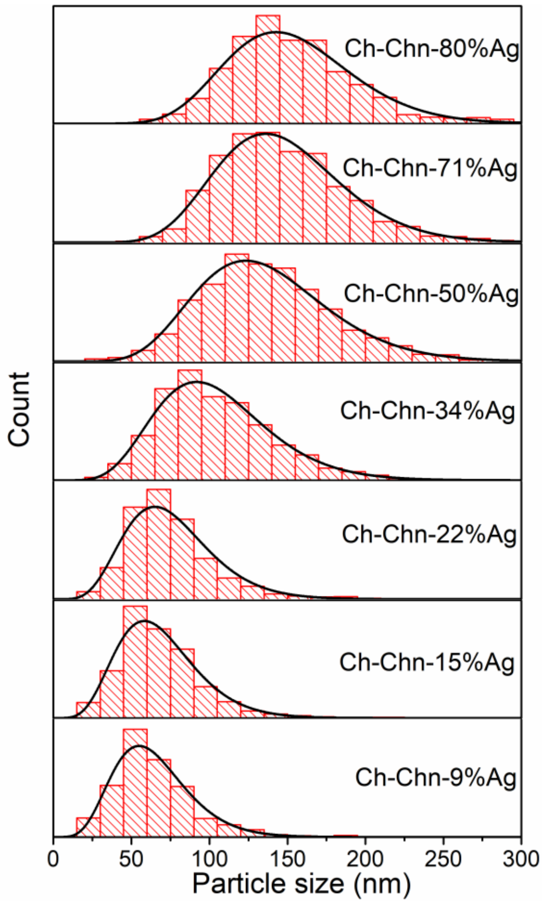

Fig. 5. Ag NPs distribution histograms for Ch-Chn-Ag NPs composites.

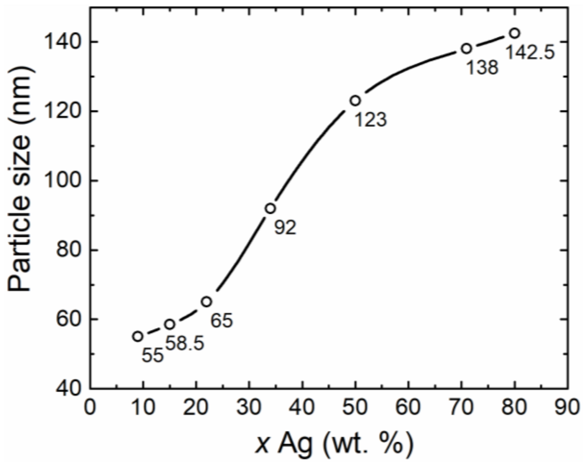

Fig. 6. Compositional dependence of the average size of Ag NPs in composites.

also estimated: Ch-Chn-Ag NPs 9% = 9.5%, Ch-Chn-Ag NPs 15% = 14%, Ch-Chn-Ag NPs 22% = 19%, Ch-Chn-Ag NPs 34% = 36%, Ch-Chn-Ag NPs 50% = 51%, Ch-Chn-Ag NPs 71% = 69% and Ch-Chn-Ag NPs 80% = 78%. This confirms the completeness of $Ag^+ \rightarrow Ag^0$ reduction in the process of preparing the composites.

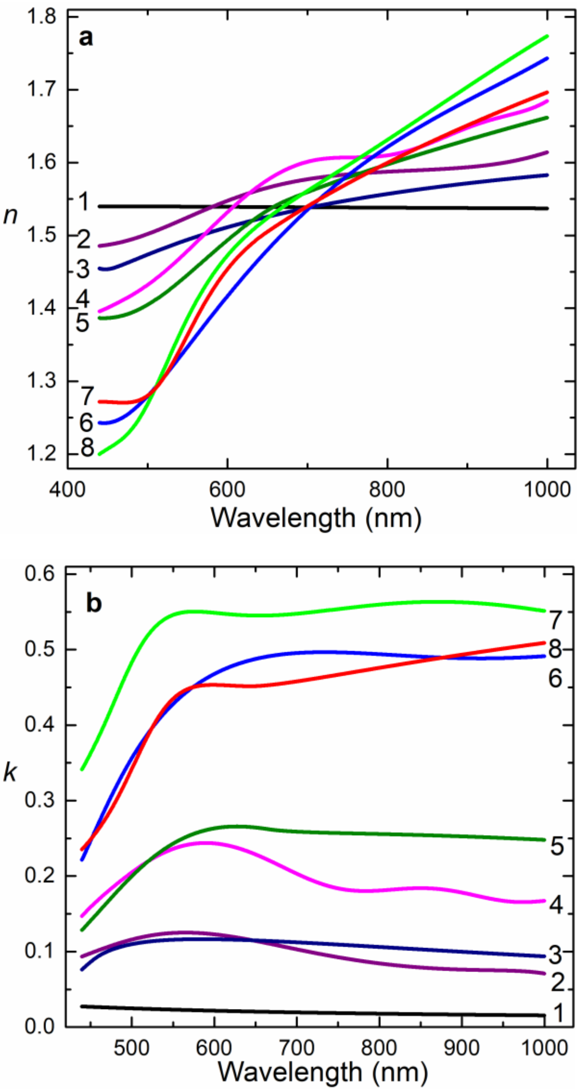

Fig. 7. Spectral dependences of the refractive index (a) and the extinction coefficient (b) dispersion: *1* – Ch-Chn, *2* – Ch-Chn-9% Ag NPs, *3* – Ch-Chn-15% Ag NPs, *4* – Ch-Chn-22% Ag NPs, *5* – Ch-Chn-34% Ag NPs, *6* – Ch-Chn-50% Ag NPs, *7* – Ch-Chn-71% Ag NPs, *8* – Ch-Chn-80% Ag NPs.

UV-VIS spectroscopy is one of the most convenient, reliable and widespread methods of characterizing nanoparticles, due to the relationship between the optical properties of nanoparticles and their size, shape, and aggregation rate [43]. UV-VIS spectra are more commonly used to characterize Au and Ag NPs, since a feature of the optical properties of metal and metal-semiconductor nanostructures is localized surface plasmon resonance (LSPR) [44]. LSPR manifests itself in a sharp increase in the absorption and scattering of electromagnetic radiation by nano-objects at a certain wavelength of the incident light, which falls into resonance with the natural frequency of electron gas oscillations on the surface of the nanostructure. It is known that the intensity, half-width of the peak and the position on the spectral scale of the plasmon resonance of nanostructures mainly depend on the material and geometric parameters (shape, size, structure).

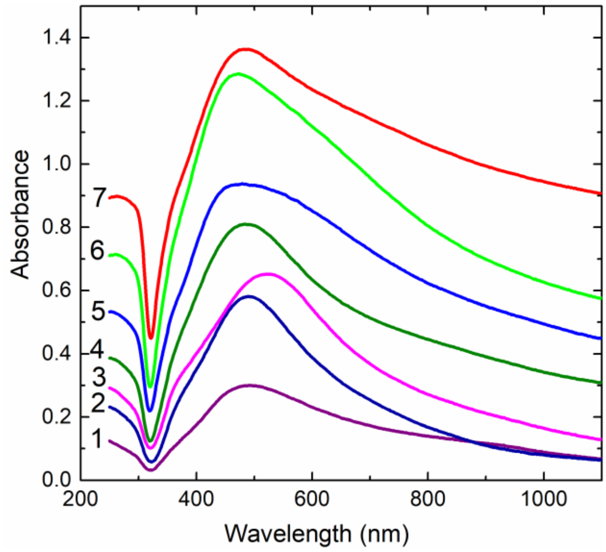

Fig. 8. Absorption spectra of Ch-Chn-Ag NPs composites: *1* – Ch-Chn-9% Ag NPs, *2* – Ch-Chn-15% Ag NPs, *3* – Ch-Chn-22% Ag NPs, *4* – Ch-Chn-34% Ag NPs, *5* – Ch-Chn-50% Ag NPs, *6* – Ch-Chn-71% Ag NPs, *7* – Ch-Chn-80% Ag NPs.

The optical absorption spectra (Fig. 8) of Ch-Chn-Ag NPs composites are characterized by the presence of an absorption maximum within the region of 458 to 525 nm. The absorption region is caused by the Mie plasmon resonance characteristic of noble metals. It was established that with an increase in the diameter of the silver nanospheres from 55 to 143 nm, the absorption peak expands significantly. It is noteworthy that in the concentration range of 9 to 22 wt.% Ag^0 (Fig. 8, curve *1*–*3*), the displacement of the absorption maximum occurs to the low-energy (long-wave) side, while the further increase in the silver content leads to a change in the position of this maximum in the high-energy (short-wave) area (Fig. 8, curves *3*–*7*). It is known that this behavior, that is a proportional shift of the absorption maximum depending on the increase in the size of the nanospheres to the low-energy (long-wave) region (9…22 wt.% Ag^0) is characteristic of the spectra of nanocomposites in which the size of the nanoparticles lies within ~ 100 nm. This is in good agreement with the relatively narrow range of distribution of particles (Fig. 5), their average size (Figs 5 and 6) and literature data on the absorption spectra of small concentrations of silver nanoparticles [44]. The shift of the absorption peaks to the high-energy (short-wave) region observed in the absorption spectra of nanocomposites with a higher concentration of silver nanoparticles (> 22 wt.%) is possibly related to further formation of nanostructures on the existing nuclei with a partial change in morphology, which explains the gradual broadening of the absorption peak. That is, formation of more complex (aggregated) nanostructures is possible.

In addition, in the absorption spectra, we observed formation of an additional weak absorption region around 350 nm. It should be noted that the authors of [45] explain the formation of an additional absorption maximum due to the appearance of quadrupole plasmon resonance with an increase in the size of silver nanospheres.

For a more detailed analysis of the optical spectra of the obtained nanocomposites, it is advisable to use the absorption coefficient (α), which was determined by the relation (5):

$$\alpha = -\frac{1}{d} \times \ln \frac{1}{T\%}, \qquad (5)$$

where d is the thickness of the film sample in cm, T is transmittance [46]. The thickness of Ch-Chn-Ag NPs composite film samples determined by the method of optical ellipsometry was used for the calculations.

The spectral dependences of the absorption coefficient α are nonlinear for all the studied composites, which is manifested by the presence of a maximum and a minimum in the energy regions around 2.5 and 3.7 eV, respectively. Since the absorption coefficient α takes into account the thickness of the sample, it allows to estimate the transmittance of samples with different thicknesses. As it can be seen from Fig. 9a, the transmittance of Ch-Chn-Ag NPs composites decreases with increasing the Ag^0 content. Further, the obtained absorption coefficient was used to calculate the energy of optical transitions by using the Tauc method.

We used the Tauc method, Eq. (6), for detailed optical characterization of silver nanoparticles:

$$(\alpha h\nu)^2 = A(h\nu - E_g), \qquad (6)$$

where α is the absorption coefficient at each wavelength, h is Planck's constant, ν is the photon frequency, E_g is the energy of the optical transition, A is the proportionality constant, degree 2 indicates the nature of the optical electronic transition – direct allowed, which is characteristic of noble metal nanoparticles [45].

The values of energies of optical transitions can be obtained from the graphical dependence by Tauc $(\alpha h\nu)^2 - f(h\nu)$, which was constructed for nanocomposite films with different concentration of silver nanoparticles (Fig. 9b).

Let us consider the spectral dependences of the absorption coefficient $(\alpha h\nu)^2 - f(h\nu)$. For Ch-Chn-Ag NPs with the Ag concentration 9 wt.%, one linear section is observed on the Tauc plot (Fig. 9, curve *2*). An increase in the concentration of Ag nanoparticles in the composites, starting with the composition of 15 wt.% Ag (Fig. 9, curve *2*), leads to the appearance of two linear sections of the spectrum, the clarity of which increases with an increase in the concentration of silver in the composites (Fig. 9, curves *2*–*7*). The gradual appearance of two linear sections may be caused by dynamics of formation of Ag^0 aggregates, the change in the morphology of the composite/nanostructure, and is obviously related to the increase in the average size of nanoparticles (Fig. 6) with the simultaneous expansion of their distribution range (Fig. 5).

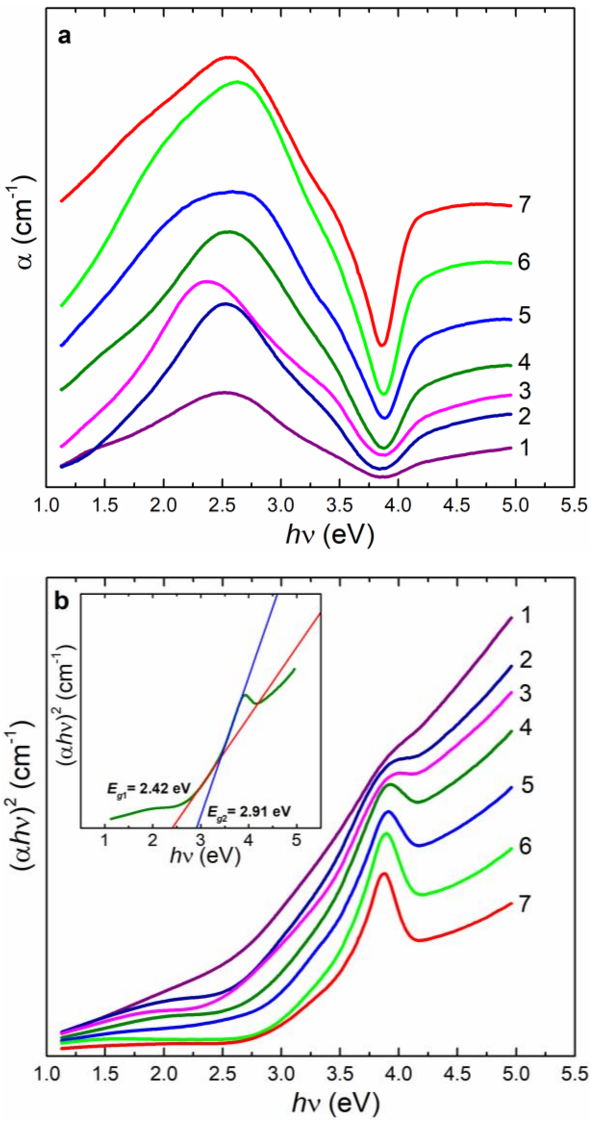

Fig. 9. Spectral dependence of the absorption coefficient α (a) and Tauc plots (b) of Ch-Chn-Ag NPs composites, the inset (b) shows determination of local plasmon and quadrupole resonance energies on the example of the Ch-Chn-Ag NPs composite (34% Ag): *1* – Ch-Chn-9% Ag NPs, *2* – Ch-Chn-15% Ag NPs, *3* – Ch-Chn-22% Ag NPs, *4* – Ch-Chn-34% Ag NPs, *5* – Ch-Chn-50% Ag NPs, *6* – Ch-Chn-71% Ag NPs, *7* – Ch-Chn-80% Ag NPs.

As a result of the analysis with the application of Tauc's method and processing of the linear parts of the spectra by using the least squares function, the values of the local (E_{g1}) and quadrupole (E_{g2}) plasmon resonance energies of the optical transitions were found (Fig. 10).

As it is known, silver NPs reveal strong plasmonic features [19]. It appears due to interaction of light photons with the surface, rather with outer free electrons of NPs. As a result of light and outer electrons interaction, the so-called surface plasmon resonance is observed. Since this phenomenon is surface-related, the surface plasmon resonance strongly depends on particle dimensional characteristics. So, the size of the particle determines the absorption peak position. In addition, an important factor affecting plasmon resonance is the matrix that surrounds Ag NPs. It is related with electron density donation between Ag NPs and organic matrix.

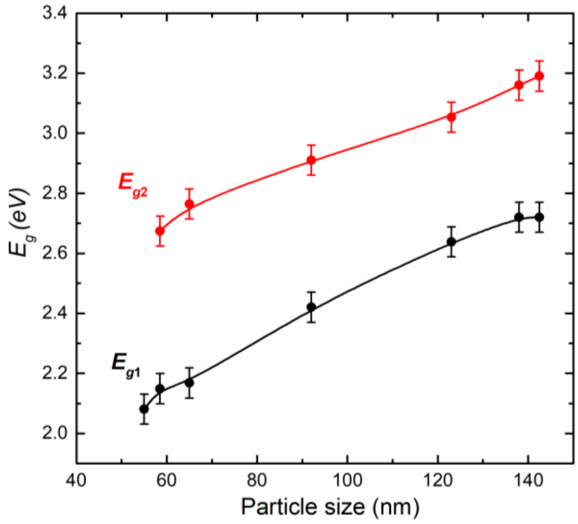

Fig. 10. Dependence of the energies of optical transitions of local (E_{g1}) and quadrupole (E_{g2}) plasmon resonances on the size of silver nanoparticles.

It was established that, as the size of the nanoparticles increases (from 55 to 143 nm), both of plasmon resonance energies (E_{g1} and E_{g2}) shift to blue side. It should be mentioned, that the dependence of the optical transition energies on the particle size is typical for silver nanoparticles [47]. Since the polymer matrix is the same for all the films, the change in plasmon resonance energies is directly related to the particle size. This is caused by the fact that with increasing the Ag NPs size the scattering ability of electrons decreases. As a result, a blue shift of the surface plasmon resonance is observed.

4. Conclusions

As a result of this study, the high-quality chitosan-chitin copolymer/Ag nanocomposite films were prepared in a wide concentration range of 9 to 80 wt.% Ag NPs. The silver nanoparticles were obtained by the direct chemical reduction of Ag^+ ions with ascorbic acid in a previously prepared chitosan solution. Formation of a chitin-chitosan copolymer, which acts as a polymer matrix for Ag NPs, was determined using the results of X-ray diffraction and FTIR studies. The complete recovery of silver and formation of Ag NPs with different sizes were confirmed by the X-ray diffraction and spectral ellipsometry methods. The morphology and distribution of Ag NPs in the polymer matrix were studied using the SEM analysis. It was ascertained that the formed metal NPs are spherical in shape, the size of which increases with an increased concentration of Ag^+ ions in the reaction mixtures. The change in the size of Ag NPs is also confirmed by the change in the width of the diffraction peaks corresponding to silver particles. All the films are characterized by a uniform distribution of Ag NPs in the polymer matrix. It was determined that the average size of Ag NPs increases from 55 nm (9 wt.%) up to 143 nm (80 wt.%), and a monotonous non-linear increase in particle size is observed on the concentration dependence of the average crystallite size. This is related to the different tendency to aggregation with increasing silver concentration and is caused by the decrease in the distance between silver particles in the polymer matrix.

Using UV-VIS spectroscopy and spectral ellipsometry methods the optical properties of the Ch-Chn-Ag NPs films were studied. An increase in the values of the refractive index and the extinction coefficient with an increase in the content of silver in the polymer is observed. The dispersion of refractive index and the extinction coefficient of the films are characterized by the presence of a slight maximum in the spectral range 500…700 nm. The obtained optical absorption spectra of chitosan-chitin copolymer/Ag composites are characterized by a typical absorption maximum in the 458…525 nm region. An increase in the peak area with an increase in the diameter of the silver nanospheres from 55 to 143 nm was observed. It was ascertained that in the low Ag concentration region (9…22 wt.%) the absorption maximum shifts to the low-energy region, while in more concentrated one (34…80 wt.%) the absorption maximum shifts to the high-energy region. This behavior of nanocomposites is associated with a change in the size of Ag NPs and formation of more complex nanostructured aggregates in highly concentrated samples. Using Tauc's method, the energies of optical transitions of Ag NPs in the obtained films were calculated. It was found that the values of energies inherent to optical transitions, which correspond to local and quadrupole surface plasmon resonances, in the process of increasing the average nanoparticle size from 55 to 143 nm are characterized by a tendency to monotonous growth.

Acknowledgements

The work at P.J. Šafarik University was supported by the grant of the Slovak Research and Development Agency under the contract (APVV-20-0324) and by the National Scholarship Programme of the Slovak Republic (Grant ID 39133). The authors would also thank the Armed Forces of Ukraine for providing security to perform this work. This work has become possible only because resilience and courage of the Ukrainian Army.

References

1. Khan I., Saeed K., Khan I. Nanoparticles: Properties, applications and toxicities. *Arab. J. Chem.* 2019. **12**. P. 908–931. https://doi.org/10.1016/j.arabjc.2017.05.011.
2. Baig N., Kammakakam I., Falath W. Nanomaterials: a review of synthesis methods, properties, recent progress, and challenges. *Mater. Adv.* 2021. **2**. P. 1821–1871. http://doi.org/10.1039/D0MA00807A.
3. Mitchell M.J., Billingsley M.M., Haley R.M. *et al.* Engineering precision nanoparticles for drug delivery. *Nat. Rev. Drug Discov*. 2021. **20**. P. 101–124. https://doi.org/10.1038/s41573-020-0090-8.
4. Harish V., Tewari D., Gaur M. *et al.* Review on nanoparticles and nanostructured materials: Bioimaging, biosensing, drug delivery, tissue engineering, antimicrobial, and agro-food applications. *Nanomater.* 2022. **12**, No 3. P. 457. https://doi.org/10.3390/nano12030457.
5. Singh T., Shukla S., Kumar P. *et al.* Application of nanotechnology in food science: Perception and overview. *Front. microbiol.* 2017. **8**. P. 2517. https://doi.org/10.3389/fmicb.2017.01501.
6. Aflori M. Smart nanomaterials for biomedical applications – A review. *Nanomater.* 2021. **11**, No 2. P. 396. https://doi.org/10.3390/nano110203967.
7. Yaqoob A.A., Ahmad H., Parveen T. *et al.* Recent advances in metal decorated nanomaterials and their various biological applications: A review. *Front. chem.* 2020. **8**. P. 341. https://doi.org/10.3389/fchem.2020.00341.
8. Yaqoob A.A., Umar K., Ibrahim M.N.M. Silver nanoparticles: Various methods of synthesis, size affecting factors and their potential applications – a review. *Appl. Nanosci*. 2020. **10**. P. 1369–1378. https://doi.org/10.1007/s13204-020-01318-w.
9. Jan H., Gul R., Andleeb A. *et al.* A detailed review on biosynthesis of platinum nanoparticles (PtNPs), their potential antimicrobial and biomedical applications. *J. Saudi Chem. Soc*. 2021. **25**(8). P. 101297. https://doi.org/10.1016/j.jscs.2021.101297.
10. Hu X., Zhang Y., Ding T. *et al.* Multifunctional gold nanoparticles: A novel nanomaterial for various medical applications and biological activities. *Front. bioeng. biotechnol.* 2020. **8**. P. 990. https://doi.org/10.3389/fbioe.2020.00990.
11. Al-Hakkani M.F. Biogenic copper nanoparticles and their applications: A review. *SN Appl. Sci*. 2020. **2**. P. 505. https://doi.org/10.1007/s42452-020-2279-1.
12. Alex K.V., Pavai P.T., Rugmini R. *et al.* Green synthesized Ag nanoparticles for bio-sensing and photocatalytic applications. *ACS Omega.* 2020. **5**. P. 13123–13129. https://doi.org/10.1021/acsomega.0c01136.
13. Crisan C.M., Mocan T., Manolea M. *et al.* Review on silver nanoparticles as a novel class of antibacterial solutions. *Appl. Sci.* 2021. **11**, No 3. P. 1120. https://doi.org/10.3390/app11031120.
14. Che W., Xiao Z., Wang Z. *et al.* Wood-based mesoporous filter decorated with silver nanoparticles for water purification. *ACS Sustain. Chem. Eng.* 2019. **7**. P. 5134–5141. https://doi.org/10.1021/acssuschemeng.8b06001.
15. Montes-Hernandez G., Di Girolamo M., Sarret G. *et al.* In situ formation of silver nanoparticles (Ag-NPs) onto textile fibers. *ACS Omega*. 2021. **6**. P. 1316–1327. https://doi.org/10.1021/acsomega.0c04814.
16. Fernandes I.J., Aroche A.F., Schuck A. *et al.* Silver nanoparticle conductive inks: synthesis, characterization, and fabrication of inkjet-printed flexible electrodes. *Sci. Rep.* 2020. **10**. P. 8878. https://doi.org/10.1038/s41598-020-65698-3.

17. Su C., Han B., Ma J., Guo P., Xu L. Effects of silver nanoparticle on electrochemical performances of poly(o-phenylenediamine)/Ag hybrid composite as anode of lithium-ion batteries. *J. Solid State Electrochem*. 2020. **24**. P. 1007–1015. https://doi.org/10.1007/s10008-020-04580-8.
18. Fizer M.M., Mariychuk R.T., Fizer O.I. Gold nanoparticles green synthesis with clove oil: spectroscopic and theoretical study. *Appl. Nanosci.* 2020. **12.** P. 611–620. https://doi.org/10.1007/s13204-021-01726-6.
19. Mariychuk R., Smolková R., Bartošová V. *et al*. The regularities of the *Mentha piperita* L. extract mediated synthesis of gold nanoparticles with a response in the infrared range. *Appl. Nanosci.* 2022. **12**. P. 1071–1083. https://doi.org/10.1007/s13204-021-01740-8.
20. Siddiqi K.S., Husen A., Rao R.A.K. A review on biosynthesis of silver nanoparticles and their biocidal properties. *J. Nanobiotechnology*. 2018. **16**. P. 14. https://doi.org/10.1186/s12951-018-0334-5.
21. Marks L.D., Peng L. Nanoparticle shape, thermodynamics and kinetics. *J. Phys.: Condens. Matter*. 2016. **28**. P. 053001. https://doi.org/10.1088/0953-8984/28/5/053001.
22. Kang H., Buchman J.T., Rodriguez R.S. *et al*. Stabilization of silver and gold nanoparticles: Preservation and improvement of plasmonic functionalities. *Chem. Rev.* 2019. **119**. P. 664–699. https://doi.org/10.1021/acs.chemrev.8b00341.
23. Javed R., Zia M., Naz S. *et al*. Role of capping agents in the application of nanoparticles in biomedicine and environmental remediation: recent trends and future prospects. *J. Nanobiotechnology*. 2020. **18.** P. 172. https://doi.org/10.1186/s12951-020-00704-4.
24. Qadir A., Le T.K., Malik M. *et al*. Representative 2D-material-based nanocomposites and their emerging applications: a review. *RSC Adv.* 2021. **11**. P. 23860–23880. https://doi.org/10.1039/D1RA03425A.
26. Mohammed A.S.A., Naveed M., Jost N. Polysaccharides; classification, chemical properties, and future perspective applications in fields of pharmacology and biological medicine (a review of current applications and upcoming potentialities). *J. Polym. Environ*. 2021. **29.** P. 2359–2371. https://doi.org/10.1007/s10924-021-02052-2.
27 Isobe N., Kaku Y., Okada S. *et al*. Identification of chitin allomorphs in poorly crystalline samples based on the complexation with ethylenediamine. *Biomacromolecules*. 2022. **23.** P. 4220–4229. https://doi.org/10.1021/acs.biomac.2c00714.
28. Pighinelli L., Broquá J., Zanin B.G. *et al*. Methods of chitin production a short review. *Am. J. Biomed. Sci. & Res*. 2019. **3**, No 4. P. 307–314. https://doi.org/10.34297/AJBSR.2019.03.000682.
29. Joseph S.M., Krishnamoorthy S., Paranthaman R. *et al*. A review on source-specific chemistry, functionality, and applications of chitin and chitosan. *Carbohydrate Polymer Technologies and Applications*. 2021. **2**. P. 100036. https://doi.org/10.1016/j.carpta.2021.100036.
30. Kravanja G., Primožič M., Knez Ž., Leitgeb M. Chitosan-based (nano)materials for novel biomedical applications. *Molecules*. 2019. **24**. P. 1960. https://doi.org/10.3390/molecules24101960.
31. Morsi R.E., Alsabagh A.M., Nasr S.A., Zaki M.M. Multifunctional nanocomposites of chitosan, silver nanoparticles, copper nanoparticles and carbon nanotubes for water treatment: Antimicrobial characteristics. *Int. J. Boil. Macromol.* 2017. **97**. P. 264–269. https://doi.org/10.1016/j.ijbiomac.2017.01.032.
32. Botelho C.M., Fernandes M.M., Souza J.M. *et al*. New textile for personal protective equipment – plasma chitosan/silver nanoparticles nylon fabric. *Fibers*. 2021. **9**. P. 3. https://doi.org/10.3390/fib9010003.
33. Ahmed S., Nirala R.K., Kumar R., Ikram S. Green synthesis of chitosan/nanosilver hybrid bionanocomposites with promising antimicrobial, antioxidant and anticervical cancer activity. *Polym. Polym. Compos.* 2021. **29**. P. S199–S210. https://doi.org/10.1177/0967391121993977.
34. Qin H., Li J., He B. *et al*. Novel wearable electrodes based on conductive chitosan fabrics and their application in smart garments. *Materials*. 2018. **11**. P. 370. https://doi.org/10.3390/ma11030370.
35. Xing L., Zhao Q., Zheng X. *et al*. Porous Ag-chitosan nanospheres bridged by cysteine residues for colorimetric sensing of trace Hg^{2+}. *ACS Appl. Nano Mater.* 2021. **4**. P. 3639–3646. https://doi.org/10.1021/acsanm.1c00157.
36. Artunduaga Bonilla J.J., Honorato L., Guimarães A.J. *et al*. Silver chitosan nanocomposites are effective to combat sporotrichosis. *Front. nanotechnol*. 2022. **4**. P. 857681. https://doi.org/10.3389/fnano.2022.857681.
37. Malakhovska T.O., Pogodin A.I., Filep M.J. *et al*. Optical characteristics of silver-based nanocomposites fabricated by an environmentally friendly method. *SPQEO*. 2023. **26**. P. 76–83. https://doi.org/10.15407/spqeo26.01.076.
38. Essel T.Y., Koomson A., Seniagya M.P.O. *et al*. Chitosan composites synthesized using acetic acid and tetraethylorthosilicate respond differently to methylene blue adsorption. *Polymers*. 2018. **10.** P. 466. https://doi.org/10.3390/polym10050466.
39. Argüelles-Monal W.M., Lizardi-Mendoza J., Fernández-Quiroz D. *et al*. Chitosan derivatives: Introducing new functionalities with a controlled molecular architecture for innovative materials. *Polymers*. 2018. **10**. P. 342. https://doi.org/10.3390/polym10030342.
40. Carlstrom D. The crystal structure of α-chitin (poly-n-acetyl-d-glucosamine). *J. Cell Biol.* 1957. **3.** P. 669–683. https://doi.org/10.1083/jcb.3.5.669.

41. Mo F., Jensen L.H. A refined model for N-acetyl-α-d-glucosamine. *Acta Crystallogr. B.* 1975. **31**. P. 2867–2873. https://doi.org/10.1107/S0567740875009077.
42. Carlberg M., Pourcin F., Margeat O. *et al*. Spectroscopic ellipsometry study of silver nanospheres and nanocubes in thin film layers. *Opt. Mater. Express.* 2017. **7**. P. 4241–4248. https://doi.org/10.1364/OME.7.004241
43. Amendola V., Meneghetti M. Size evaluation of gold nanoparticles by UV−vis spectroscopy. *J. Phys. Chem*. 2009. **113**. P. 4277–4285. https://doi.org/10.1021/jp8082425.
44. Meikhail M.S., Abdelghany A.M., Aldhabi A.A. Preparation and characterization of silver and gold nanoparticles and study influence on physical properties of PVA/PVP nanocomposites. *J. Adv. Phys.* 2017. **13**. P. 4628–4639. https://doi.org/10.24297/jap.v13i1.5626.
45. Amirjani A., Koochak N.N., Haghshenas D.F. Synthesis of silver nanotriangles with tunable edge length: A promising candidate for light harvesting purposes within visible and near-infrared ranges. *Mater. Res. Express*. 2018. **6**. P. 036204. https://doi.org/10.1088/2053-1591/aaf624.
46. Filep M., Molnár K., Sabov M., Csoma Z., Pogodin A. Structural, thermal, and optical properties of Co^{2+} and Mg^{2+} doped $K_2Ni(SO_4)_2{\cdot}6H_2O$ single crystals. *Opt. Mater.* 2021. **122A**. P. 111753. https://doi.org/10.1016/j.optmat.2021.111753.
47. Yeshchenko O.A., Dmitruk I.M., Alexeenko A.A. *et al*. Size and temperature effects on the surface plasmon resonance in silver nanoparticles. *Plasmonics.* 2012. **7**. P. 685–694. https://doi.org/10.1007/s11468-012-9359-z.

Authors and CV

Tetyana O. Malakhovska, defended her PhD thesis in inorganic chemistry in 2010. Senior researcher at the Uzhhorod National University. Authored 70 articles and 10 patents. The area of her scientific interests includes solid state chemistry and materials science.
E-mail: t.malakhovska@gmail.com,
https://orcid.org/0000-0001-7309-4894

Artem I. Pogodin, defended his PhD thesis in Inorganic Chemistry in 2016. Senior Researcher at the Uzhhorod National University. Authored over 100 scientific articles and 114 patents. The area of his scientific interests includes solid state chemistry, crystal growth and materials science.
E-mail: artempogodin88@gmail.com,
https://orcid.org/0000-0002-2430-3220

Mykhailo J. Filep, PhD in Inorganic Chemistry, Senior Researcher at the Uzhhorod National University, Associate professor at the Ferenc Rákóczi II Transcarpathian Hungarian Institute. Authored over 100 articles and 50 patents. The area of his scientific interests includes solid state chemistry and materials science.
E-mail: mfilep23@gmail.com,
http://orcid.org/0000-0001-7017-5437

Ruslan Mariychuk, PhD, is an associate professor at the Department of Ecology, University of Presov, Presov, Slovakia. Author of over 60 publications indexed in Scopus and Web of Science databases and 3 patents. His research interests include green chemistry, sustainable synthesis of nanomaterials, and materials science.
E-mail: ruslan.mariychuk@unipo.sk,
https://orcid.org/0000-0001-8464-4142

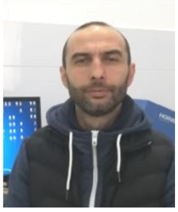

Mykhailo M. Pop, defended his PhD thesis in Physics and Mathematics in 2016. Lecturer and Researcher at the Uzhhorod National University, Ukraine. Authored of nearly 100 publications. The area of his scientific interests includes physical and optical properties of semiconductors, superionic materials, chalcogenide glasses and films.
E-mail: mykhaylo.pop@uzhnu.edu.ua,
https://orcid.org/0000-0003-3674-3482

Yaroslav I. Studenyak, PhD, is an associate professor at the Department of Analytical Chemistry, Uzhhorod National University. Author of over 20 publications indexed in Scopus and Web of Science databases and 9 patents.
E-mail: yaroslav.studenyak@uzhnu.edu.ua,
https://orcid.org/0000-0002-8970-2222

Vasyl V. Vakulchak, defended his PhD thesis in Physics and Mathematics in 2015. Senior researcher of the Department of Applied Physics at the Uzhhorod National University. Authored over 80 scientific publications and 1 patent. The area of scientific interest is an *ab-initio* calculation of the electronic structure, physical properties of semiconductors.
E-mail: vasyl.vakulchak@uzhnu.edu.ua,
https://orcid.org/0000-0001-6037-8978

Vladimir Komanicky, defended his PhD thesis in Chemistry in 2003 at the University of California. He is a leading scientist of electrocatalysis and nanotechnology group at the Institute of Physics at P.J. Safarik University in Kosice. He is author of 107 publications, 2 patents, and 2 textbooks. The area of his scientific interests includes nanotechnology, electrocatalysis, semiconductor physics, magnetism and superconductivity.
E-mail: vladimir.komanicky@upjs.sk,
https://orcid.org/0000-0001-8649-1987

Serhii Vorobiov, defended his PhD thesis in Physics and Mathematics in 2015 at Sumy State University, Ukraine. Postdoctoral researcher of the Institute of Physics, Faculty of Science, P.J. Safarik University, Slovakia. Author of 46 publications indexed in Scopus and Web of Science databases and 1 patent. The area of his scientific interests includes nanofabrication and thin film technology, magnetic and magnetoresistance properties nano and mesoscopic systems.
E-mail: serhii.vorobiov@upjs.sk,
https://orcid.org/0000-0002-5884-3292

Marian Y. Sabov, defended his PhD thesis in inorganic chemistry in 2000. Associate professor at the Uzhhorod National University (Department of Inorganic Chemistry). Authored over 100 articles and 35 patents. The area of his scientific interests includes solid state chemistry and materials science.
E-mail: marian.sabov@uzhnu.edu.ua,
https://orcid.org/0000-0003-0346-0734

Authors' contributions

Malakhovska T.O.: supervision, conceptualization, investigation, writing – original draft.
Pogodin A.I.: investigation, visualization, validation, writing – original draft.
Filep M.J.: investigation, writing – original draft.
Mariychuk R.: writing – review & editing.
Pop M.M.: investigation, writing – review & editing.
Studenyak Ya.I.: methodology, visualization.
Vakulchak V.V.: investigation, visualization.
Komanicky V.: methodology, writing – review & editing.
Vorobiov S.: methodology, visualization.
Sabov M.Yu.: methodology, visualization.

Структурні та оптичні характеристики тонких плівок нанокомпозитів хітозан-хітин/Ag

Т.О. Малаховська, А.І. Погодін, М.Й. Філеп, Р. Марійчук, М.М. Поп, Я.І. Студеняк, В.В. Вакульчак, В. Команіцкі, С. Воробйов, М.Ю. Сабов

Анотація. Хітин та його похідні є поширеними природними полімерами, які широко використовуються в різних технологічних галузях. В останні роки значна увага приділяється отриманню полімерних нанокомпозитів на основі наночастинок металів. Композити на основі хітину/хітозану завдяки високій антибактеріальній активності придатні для застосування в суміжних галузях харчової та текстильної промисловості. У даній роботі представлено ефективний і простий метод отримання нанокомпозитів на основі сополімеру хітозан-хітин/Ag з високим вмістом наночастинок металів. Структуру та морфологію синтезованих нанокомпозитів досліджено методами рентгенівської дифрактометрії, інфрачервоної спектроскопії та електронної мікроскопії, а оптичні властивості – методами оптичної спектроскопії та еліпсометрії. Установлено, що отримані нанокомпозитні плівки характеризуються рівномірним розподілом сферичних наночастинок срібла, розміри яких зростають (від 55 до 143 нм) зі збільшенням концентрації іонів Ag^+ у реакційній суміші. Оптичні спектри поглинання нанокомпозитів характеризуються наявністю максимуму поглинання в області 458…525 нм, що підтверджує утворення наночастинок срібла. Встановлено монотонне зростання значень енергій оптичних переходів у процесі збільшення середнього розміру наночастинок.

Ключові слова: нанокомпозит, хітозан, хітин, оптичні властивості, електронна мікроскопія, рентгеноструктурний аналіз.